Shear-induced particle migration in viscous suspensions with continuous size distribution

O. M. Lavrenteva, I. Smagin, and A. Nir
Faculty of Chemical Engineering, Technion, Israel Institute of Technology, Haifa, Israel

(Received 21 May 2023; accepted 17 January 2024; published 20 February 2024)

We present an approach to study the shear-induced diffusion of particles in suspensions with continuous particle-size distribution by addressing the migration of local moments of the size distribution. This approach replaces studying fluxes of particles of particular sizes. The physical problem is redefined in terms of fluxes of moments and their conservation. Particle-size distribution at each point is consequently obtained from the resulting moments, by solving inverse problems locally. The approach is applicable to any composite suspension, depending only on the initial size distribution in it. A particular example of migration in a circular tube is described. Results include concentration inhomogeneity, moments' distribution, and the consequent local continuous particle-size distributions. We present stationary physical flow parameters and the similarity and difference from cases of monodispersed suspensions. For example, while in most cases of particle concentration, the general phenomena resemble the migration directions observed in monodisperse suspensions, there are cases, associated with extreme input high or low concentrations, where further accumulation of specific sizes at locations close to domain boundaries are encountered. This basic study will enhance better understanding of the complex behavior and properties of multiphase systems.

DOI: 10.1103/PhysRevFluids.9.024305

I. INTRODUCTION

Suspensions, containing particles dispersed in a fluid, are abundant in nature and are also common in industrial processes. Some of these mixtures contain particles of nearly uniform size (monodisperse). However, many of those encountered in man-made processes contain particles having various sizes, either discrete (multidisperse) or exhibiting a continuous size distribution (polydisperse). Examples embrace slurries in chemical processes, mixtures in pharmaceutical industries, particles produced in suspension polymerization, mixtures intended to create solid fuels or explosives, and others. When the suspending fluid was Newtonian it was, historically, customary to consider the suspension as an equivalent Newtonian fluid having effective properties that depend on the phases' properties and on the partial volume fraction of the particles. Thus, according to this oversimplified approach, when such a suspension was to be processed, e.g., pumped in a tube, the effective viscosity would have dictated the power needed to sustain this flow. This paper addresses flow of such suspensions, which are composed of particles with a continuous size distribution.

Phenomena encountered in operations with such systems suggested that the *a priori* consideration of the suspension as an effective Newtonian fluid, having constant effective properties, was not preserved even for highly idealized systems with spherical particles of uniform size. We mention here a few examples. Karnis *et al.* [1] observed a drift of neutrally buoyant monodisperse spherical particles toward the center of a tube that resulted in a higher concentration there. Gadala-Maria and Acrivos [2] and Leighton and Acrivos [3] reported a dynamic reduction of the measured effective viscosity of a monodisperse suspension of spherical particles when sheared in a Couette cell. More recent papers include apparent wall slip in the processing of dense pastes (Kalyon [4,5]).

In multidisperse systems the processing resulted in separation and segregation of sizes, e.g., reports by Abbott *et al.* [6] and Krishnan *et al.* [7]. Naturally, such inhomogeneous distribution results in local variations of bulk effective properties such as viscosity or density, and in shear dependence of the rheometric behavior of the suspension that is more characteristic of non-Newtonian systems.

Leighton and Acrivos [8] followed Eckstein *et al.* [9] and established the concept of migration of spherical particles in a suspension that is subject to shear. Each particle interacts with a huge number of neighbors, which themselves experience similar interactions, and its net resulting trajectory in the suspension is a random walk. Hence, particles in the sheared suspension exhibit a diffusion (or dispersion) induced by shear. In the absence of Brownian effects, the intensity of this diffusion is a result of two physical factors: the existence of shear and the concentration (volume fraction) of particles in the suspension. When the shear field and the particle concentration in the system are uniform, e.g., in a simple shear flow, the particles experience a self-diffusion. However, when the system contains variation in the shear field, as it is for example sheared in a Couette device or flows in a tube, and when the concentration field is not uniform, the local flux of particles is driven by the variations in these fields.

A fundamental theory to predict the diffusivity from basic principles is yet to be developed, as it confronts resolving a multibody problem of viscous interactions. Yet, several approaches based on semiempirical models permit analyses of the bulk migration processes. For simple suspensions and flow fields, these predictions were corroborated by experimental studies. Primarily, there are four types of such models:

(1) Migration is induced by a combination of shear intensity and concentration gradients [8].

(2) Migration is a result of gradients in the particle interaction frequency and the viscous field intensity (Phillips *et al.* [10]).

(3) Normal stresses and "temperature" and "osmotic pressure," defined for the suspension, dictate the migration process (Nott and Brady [11]; Leshansky *et al.* [12]).

(4) Lattice-Boltzmann method coupled with discrete method (Chun *et al.* [13]; Di Vaira *et al.* [14]).

The works mentioned in the paragraphs above were cited by numerous works on shear-induced migration and associated phenomena. Nevertheless, some focused reviews of the subject can be found (e.g., Davis [15]; Stickel and Powell [16]; Klaver and Schroen [17]; Morris [18]). In many previous studies and in this paper, use is made of the approach of Ref. [10]. It enables interesting definitions of effective diffusion coefficients and migration potentials and their gradients. It also provides a rather straightforward focus on stationary results without the need to pass through tedious temporal evolutions, the convergence of which to stationarity is extremely slow, as it is in the case encountered when suspension balance is used (see method 4 above). Kang and Mirbod [19] recently reported a use of the Phillips *et al.* [10] model that incorporates in the analysis also Brownian diffusion. Shauly *et al.* [20] demonstrated that when this model is applied to study resuspension of bidispersed suspension, the results agree well with experimental results obtained for such mixtures when sheared in a Couette device (Acrivos *et al.* [21]; Tripathi and Acrivos [22]). We note that in spite of the intensive attention given to this approach, migration in the most common system of a polydisperse suspension, having continuous size distribution, was not intensively addressed as yet.

In this paper we study the flow in a straight circular tube of a polydisperse suspension of neutrally buoyant spherical particles, having a continuous particle-size distribution. It is assumed that the particles are infinitely small and that they move with the velocity of the ambient fluid. Hence, the suspension flows as an effective viscous fluid. We report various phenomena including migration, drag reduction, distribution of particle concentration, separation of sizes, distribution of particle average size. In Sec. II we follow Shauly *et al.* [23] and formulate the migration problem for a flow in a tube in terms of distribution moments. We note here that even in the case when there are particles of many discrete different sizes, and exact initial concentration for each size is difficult to determine, then the moments approach, presented below, is not only advantageous but the only possible one so far. A stationary solution in the case of a circular tube is presented in Sec. III. Results for a particular case are then given in Sec. IV, and in Sec. V we describe our approach to obtain

local particle-size distributions in the tube cross section. A discussion is given in Sec. VI followed by conclusions in Sec. VII.

II. SHEAR-INDUCED DIFFUSION REVISITED

Consider a suspension of neutrally buoyant spherical particles flowing in a tube. We follow the formulation formulated by Phillips *et al.* [10] and the supplement suggested by Krishnan *et al.* [7] in terms of variations in streamlines' curvature compensating for changes in local normal stresses. It is assumed that when the suspension flows in a tube, the particle dispersive flux in the flow direction is negligible compared to the convective flux. Thus, particles migrate across the bulk streamlines solely by radial dispersion in the tube cross section. For a monodisperse suspension in the shear field the flux of spherical particles can be expressed in the form (see also Shauly *et al.* [23])

$$\mathbf{J} = -D\nabla P \quad \text{with} \quad P = \ln(\phi\gamma\mu^2\Re); \quad D = ka^2\gamma\phi^2. \tag{1}$$

Here, k is an $O(1)$ constant, a is the particle's radius, ϕ is the local volume concentration, γ is the local intensity of the shear rate, $\Re$ is the local streamline curvature, and μ is the local effective viscosity. It is worth noting that there have been experimental studies with results agreeing with such model predictions for various shear fields (see, e.g., Abbott *et al.* [6], Koh *et al.* [24], and Tetlow *et al.* [25]). As shown in Ref. [23], for a flow in a tube it yields velocity and particle concentration profiles that agree well with experimental measurements.

When the suspension is multidisperse, containing several discrete particle sizes a_i, with partial concentration ϕ_i, after some simplifications the flux of each fraction obtains the form ([20,23])

$$\mathbf{J}_i = -D_i\left[\nabla P_i + \left(\frac{\bar{a}}{a_i} - 1\right)\nabla(\ln\mu^2) + \left(\left(\frac{a_i}{\bar{a}}\right)^2 - 1\right)\nabla\ln\Re\right], \tag{2}$$

with $P_i = \ln(\phi_i\gamma\mu^2\Re)$ and $D_i = k\gamma\phi\phi_i\bar{a}a_i$. k is an $O(1)$ constant, not necessarily the same as in a monodispersed case. The dependence of the diffusion coefficient on the local values of the total and particular particle concentration and size is embedded explicitly in D_i.

Here, the total concentration $\phi = \sum_i \phi_i$ and the local weighted average size is $\bar{a} = (\sum_i a_i\phi_i)/\phi$. The expression in (2) reflects a collection of the interactions of any particular species with all species i in the suspension.

When the suspension is polydisperse, having spherical particles with a continuous particle-size distribution where the partial fraction of the total concentration is $d\phi = \phi(a)da$, the nth moment of this distribution is defined as

$$\Phi^{(n)} = \int_{a_{\min}}^{a_{\max}} a^n d\phi = \int_{a_{\min}}^{a_{\max}} a^n\phi(a)da. \tag{3}$$

It follows from (3) that the local total particle concentration is $\phi = \Phi^{(0)}$, and the local average particle size is $\bar{a} = \Phi^{(1)}/\Phi^{(0)}$.

In what follows we assume that inertia on the scale of the particles is negligible, and render all variables nondimensional by normalizing the distances by the tube cross-section dimension R, the particle radius by the initial average one, the velocity by its average value, and the viscosity by that of the clean fluid. The ratio $\varepsilon = \frac{\bar{a}}{R}$ is considered much smaller than 1. In the analysis below we keep the nomenclature of the dimensional variables.

Multiplying Eq. (2) by a^n and integrating over the particle-size interval yields an equation for the flux of the nth moment:

$$\mathbf{J}^{(n)} = -D^{(n)}\left(\nabla P^{(n)} + \frac{\Phi^{(1)}\Phi^{(n)}}{\Phi^{(0)}\Phi^{(n+1)}}\nabla\ln\mu^2 + \frac{\Phi^{(0)^2}\Phi^{(n+3)}}{\Phi^{(1)^2}\Phi^{(n+1)}}\nabla\ln\Re\right), \tag{4}$$

where we redefine the potential and diffusivity for each moment to be of the forms $P^{(n)}(a) = \ln(\Phi^{(n+1)}\gamma)$ and $D^{(n)} = k\varepsilon^2\gamma\,\Phi^{(n+1)}\Phi^{(1)}$.

Note that the flux of moment n depends on higher moments, and that any problem emerging from (4) is associated, in principle, with an infinite number of moments.

We conclude the general formulation is concluded by introducing a dynamic equation, which is of the form $\frac{d\Phi^{(n)}}{dt} = -\nabla \cdot \mathbf{J}^{(n)}$, where $\frac{d}{dt} = \frac{\partial}{\partial t} + \mathbf{u} \cdot \nabla$, with $\mathbf{u}$ being the velocity field.

For the case of a flow of a suspension in a straight tube with circular cross section, where streamlines are straight, the term involving the gradient of streamlines curvature vanishes, and Eq. (4) simplifies to the form

$$\mathbf{J}^{(n)} = -k\varepsilon^2\Phi^{(1)}\left(\frac{d(\Phi^{(n+1)}\gamma)}{dr} + \frac{\Phi^{(1)}\Phi^{(n)}\gamma}{\Phi^{(0)}}\frac{d\ln\mu^2}{dr}\right), \tag{5}$$

with r being a cylindrical coordinate in the tube cross section.

III. STATIONARY FULLY DEVELOPED STATES OF PARTICLE MIGRATION IN A STRAIGHT CIRCULAR TUBE

Consider the flow of a suspension that was introduced to the tube with initial uniform particle concentration $\hat{\phi}$ and a parabolic velocity distribution $\hat{u}(r) = 2(1 - r^2)$. Stationary radial concentration and velocity profiles, which evolve in this flow, satisfy $\mathbf{J}^{(n)} = 0$, which in view of (5) reduces to an infinite set of ordinary differentials of the form

$$\frac{d(\Phi^{(n+1)}\gamma)}{dr} + \frac{\Phi^{(1)}\Phi^{(n)}\gamma}{\Phi^{(0)}}\frac{d\ln\mu^2}{dr} = 0 \quad \text{for each } n. \tag{6}$$

Here, $\gamma = |\frac{du}{dr}|$, with u being the stationary velocity profile, and where $\gamma = 0$ at $r = 0$ and $u = 0$ at $r = 1$. u is normalized by the initial parabolic average velocity. The natural physical boundary conditions for the infinite system of Eq. (6) are zero penetration of particles (and moments) at the tube wall. However, this adds no useful information since, at stationary state all fluxes vanish everywhere in the tube cross section. Thus, the proper requirement, additional to (6), must be preservation of all moments' fluxes, which must equal the respective fluxes at the initial introduction of the homogeneous suspension. Thus, we require

$$\int_0^1 \Phi^{(n)} u r dr = \frac{\hat{\Phi}^{(n)}}{2}, \quad n \geqslant 0, \tag{7}$$

where the term on the right-hand side is calculated using the parabolic $\hat{u}(r)$ mentioned above.

Note that there is no explicit equation for the case $n = 0$ since every equation for the nth moment involves the distribution of a higher moment, $\Phi^{(n+1)}$. For the case $n = 0$ we obtain

$$\frac{d(\Phi^{(1)}\gamma)}{dr} + \Phi^{(1)}\gamma\frac{d\ln\mu^2}{dr} = 0, \tag{8}$$

the solution of which is

$$\Phi^{(1)}\gamma\mu^2 = C, \quad \text{with } C \text{ being a constant of integration.} \tag{9}$$

A number of empirical expressions to describe the effective viscosity of a concentrated suspension with particle concentration $\Phi^{(0)}$ and maximum packing concentration ϕ_m are available in the literature; see, e.g., Pednekar *et al.* [26]. In this work we chose to use the expression suggested by Krieger [27], $\mu = \mu(\Phi^{(0)}) = (1-\frac{\Phi^{(0)}}{\phi_m})^{-1.82}$, which was obtained empirically for monodisperse suspensions where ϕ_m was estimated at 0.68. When the suspension is multidisperse, i.e., when it has several particle sizes, it is expected that ϕ_m may increase locally due to the ability of very small particles to occupy spaces between large particles. There have been studies of the effective viscosity of suspensions having particles with more than one size. (see, e.g., Krishnan and Leighton, 1995 [28] and Probstein *et al.* [29] for empirical correlation for two particle sizes). For multidisperse or for polydisperse systems with continuous size distributions, Desmond and Weeks [30] and Santos

et al. [31] suggested different dependences of ϕ_m on the first three moments of size distribution. In this work we use the constant approximation $\phi_m \approx 0.7$, being a little higher than the monodispersed limit and discuss possible effects of variable ϕ_m.

Note that from a stress balance and preservation of the total fluid flux along the tube (see Shauly *et al.*, 1998 [23]), we have

$$\gamma(r) = \frac{\frac{r}{\mu}}{\int_0^1 \frac{r^3}{\mu} dr}, \quad u(r) = \int_r^1 \gamma(r) dr, \quad \text{and} \quad \frac{dP}{dz} = \frac{1}{\int_0^1 \frac{r^3}{2\mu} dr}, \tag{10}$$

where $\frac{dP}{dz}$ is the pressure gradient along the tube.

Combining the form of the solution of (9) with the form of $\gamma(r)$ in (10), it follows that $\Phi^{(1)}$ is nonsingular near $r \to 0$ if $\gamma\mu^2 = O(1)$ and thus, γ must be of $O(r^2)$, which differs from the $O(r)$ velocity gradient in the initial state of the parabolic profile.

Furthermore, combining the singular divergence of μ at $r = 0$ with its Krieger expression $(1-\frac{\Phi^{(0)}}{\phi_m})^{-1.82}$, the particle concentration at the center of the tube must be $\Phi^{(0)} = \phi_m(0)$ and, therefore, at small r, it is of the form

$$\Phi^{(0)} = \phi_m(0) - \alpha r^{1/1.82} + o(r^{1/1.82}) \qquad r \ll 1. \tag{11}$$

(See also Appendix B in Ref. [32], for planar Poiseuille flow of monodisperse suspensions and a consequence of Eq. (24) in Ref. [23] for suspensions having several discrete sizes.)

Next, proceed to $\Phi^{(2)}$. For $\mathbf{J}^{(1)} = 0$ we require $\frac{d(\Phi^{(2)}\gamma)}{dr} = (\frac{\Phi^{(1)}}{\Phi^{(0)}})\frac{d(\Phi^{(1)}\gamma)}{dr}$. Integrating this expression yields

$$\Phi^{(2)}\gamma + \int_r^1 \left(\frac{\Phi^{(1)}}{\Phi^{(0)}}\right)\frac{d(\Phi^{(1)}\gamma)}{dr'}dr' = C_2 \quad \text{or} \quad \Phi^{(2)} = \frac{C_2 - \int_r^1 \left(\frac{\Phi^{(1)}}{\Phi^{(0)}}\right)\frac{d(\Phi^{(1)}\gamma)}{dr'}dr'}{\gamma}, \tag{12}$$

where $C_2 = (\Phi^{(2)}\gamma)(1)$. $\Phi^{(2)}(0)$ is finite if the numerator vanishes fast enough as $r \to 0$, implying that

$$C_2 = \int_0^1 \left(\frac{\Phi^{(1)}}{\Phi^{(0)}}\right)\frac{d(\Phi^{(1)}\gamma)}{dr'}dr' \quad \text{and} \quad \Phi^{(2)} = \frac{1}{\gamma}\int_0^r \left(\frac{\Phi^{(1)}}{\Phi^{(0)}}\right)\frac{d(\Phi^{(1)}\gamma)}{dr'}dr'. \tag{13}$$

By taking the limit to $r \to 0$ we find that $\Phi^{(2)}(0) = \frac{\Phi^{(1)}(0)^2}{\Phi^{(0)}(0)}$.

A similar procedure for $\Phi^{(n)}$, applying the requirement $\mathbf{J}^{(n)} = 0$, leads to the equation

$$\frac{d(\Phi^{(n+1)}\gamma)}{dr} = \left(\frac{\Phi^{(n)}}{\Phi^{(0)}}\right)\frac{d(\Phi^{(1)}\gamma)}{dr}. \tag{14}$$

And, it follows that

$$\Phi^{(n+1)}\gamma = \int_0^r \left(\frac{\Phi^{(n)}}{\Phi^{(0)}}\right)\frac{d(\Phi^{(1)}\gamma)}{dr'}dr' \quad \text{and} \quad \Phi^{(n+1)}(0) = \frac{\Phi^{(1)}(0)}{\Phi^{(0)}(0)}\Phi^{(n)}(0) \quad \text{for all } n \geqslant 1 \tag{15}$$

.

IV. A SUSPENSION HAVING INITIALLY A NORMAL PARTICLE-SIZE DISTRIBUTION

A. Distribution before migration

Results emerging from the use of the defined moments and their balances are demonstrated below. We assume that when the suspension is homogeneous, it has a uniform particle-size distribution that has a Gaussian shape.

The distribution depicted in Fig. 1 is of the form

$$\hat{\phi}(a) = ce^{-b(a-1)^2}, \quad 0 < a < 2, \quad a_{\max} = 2, \quad \hat{a} = 1. \tag{16}$$

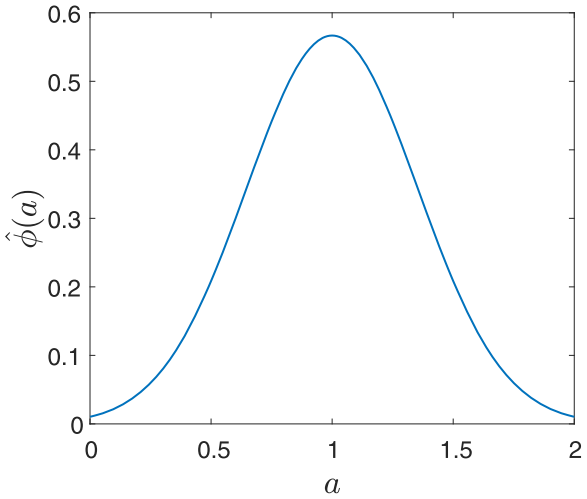

FIG. 1. A normal continuous particle-size distribution normalized by the average value.

It contains two parameters, of which b determines the span of the distribution and c is dictated in each initial case by the zero moment $\hat{\Phi}^{(0)}$. In this study we chose $b = 4$.

Higher uniform moments of the homogeneous suspension are calculated by direct integration of $\hat{\phi}(a)$ using (3). Note that there are finite partial values at the edge points of the distribution.

B. An algorithm of finding stationary solutions

Equations (6) and (7) are an infinite set that must be solved in conjunction with the auxiliary functions (9) and the Krieger effective viscosity expression, thereby providing a highly complex nonlinear system. We further recall that there is no equation for the zero moment $\Phi^{(0)}$, except for the integral preservation in (7), but that $\Phi^{(0)}$ is implicitly involved in all parts of the system. The approach we used to obtain a solution for this system is by truncating the number of moments at some large $n = N$ and replacing the preservation of fluxes in (7) by an objective function to be minimized. Thus, we look for a minimum of the functional

$$F(\Phi^{(0)}) = \sum_{n=0}^{N} \left(\int_0^1 \Phi^{(n)} u r dr - \frac{\hat{\Phi}^{(n)}}{2} \right)^2. \tag{17}$$

Furthermore, since functions in this functional are continuous in the interval $0 \leqslant r \leqslant 1$, it is beneficial to express them, the functional F and the auxiliary expressions, in terms of a common variable that is continuous in r, such as $\Phi^{(0)}$ or $\eta = 1/\mu$, that can be expressed correctly in $0 \leqslant r \leqslant 1$ by a polynomial. We choose the inverse effective viscosity as a physical candidate for such an expression and define the expansion

$$\eta = \frac{1}{\mu} = \sum_j B_j r^j, \quad \Phi^{(0)} = \phi_m (1 - \eta^{1/1.82}), \tag{18}$$

with $0 \leqslant \eta \leqslant 1$ since $\mu \to \infty$ at $r \to 0$ and $\mu = 1$ in the absence of particles.

Note that all the equations above are valid for ϕ_m that may not be constant. However, it is expected from the data collected in Ref. [26] that the augmentation of ϕ_m in polydispersed systems with normal size distribution be limited to a few percent since, in view of Fig. 1, only a small fraction of smallest particles can contribute to a change in ϕ_m. Thus, considering the distribution of sizes and the relative quantities suggested in the figure, we assume that in this study, the augmentation of ϕ_m will

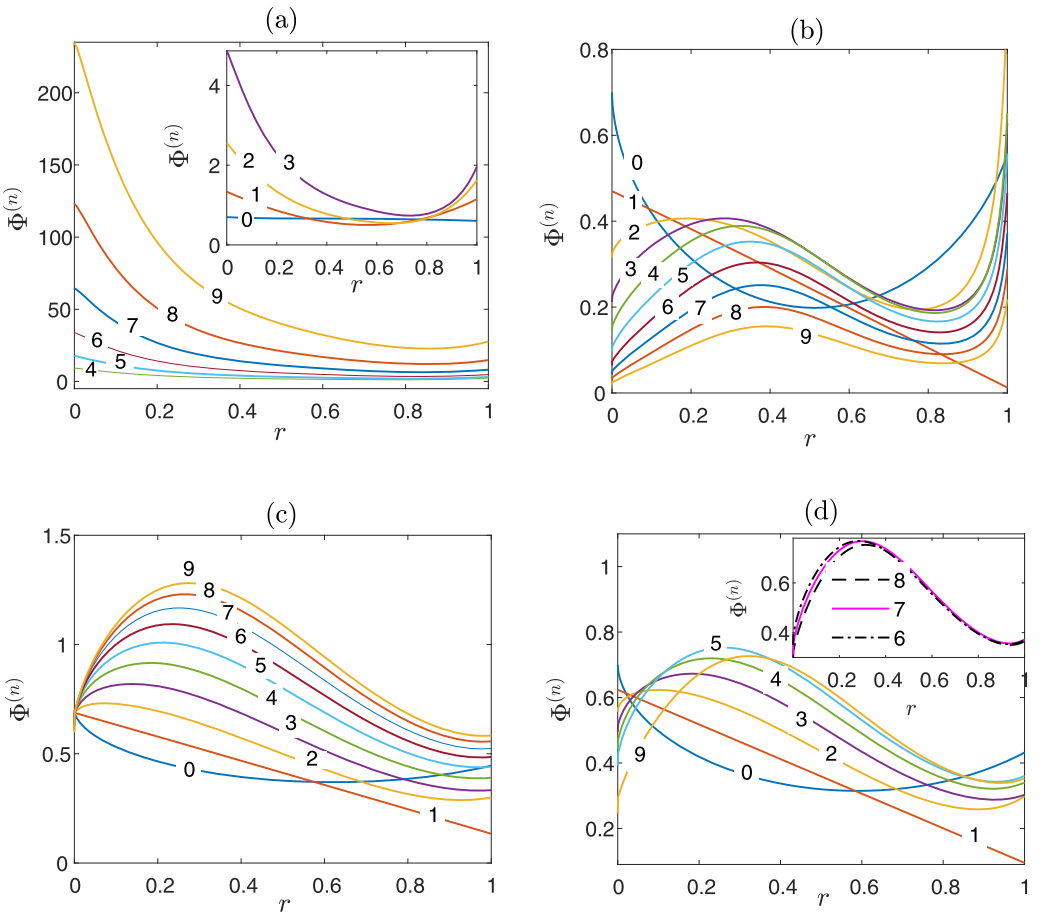

FIG. 2. Profiles of stationary moments obtained for high, low, and intermediate input particle concentration: (a) $\hat{\Phi}^{(0)} = 0.65$; (b) $\hat{\Phi}^{(0)} = 0.25$; (c) $\hat{\Phi}^{(0)} = 0.4$; (d) $\hat{\Phi}^{(0)} = 0.35$. The profiles are obtained by minimizing (17) with respect to the coefficients in the approximation (18).

be limited to a few percent, and that it is nearly uniform in r. For simplicity, we henceforth used a constant approximation $\phi_m = 0.7$. The assumption of constant ϕ_m is advantageous for the algorithm of solution, since in this case, Eq. (18) provides an explicit expression for the total concentration, which in its turn, determines all the other moments. However, in a more complex approach the above algorithm can be modified to the case of ϕ_m dependence on several moments by considering $\phi_m(0)$ as an additional constant to be found.

C. Stationary moments

We applied the algorithm described above by optimizing the values of the coefficients in the polynomial (18) to minimize the objective function (17) for the first ten moments, e.g., $\Phi^{(0)}$ to $\Phi^{(9)}$. In Fig. 2 we present example of the resulting stationary moments profiles in the tube cross section for four input cases, $\hat{\Phi}^{(0)}$, e.g., high, low, and intermediate input concentration. Evidently, in Fig. 2(a) higher moments keep increasing in size while in Fig. 2(b) higher moments keep decreasing in size, for all r. It appears that there is a transition between these states, evidently at some intermediate input concentration in the region $0.45 > \hat{\Phi}^{(0)} > 0.35$ [see Figs. 8(c) and 8(d) for depiction]. Further evidence for this transition is also discussed with respect to other results reported below. Note that

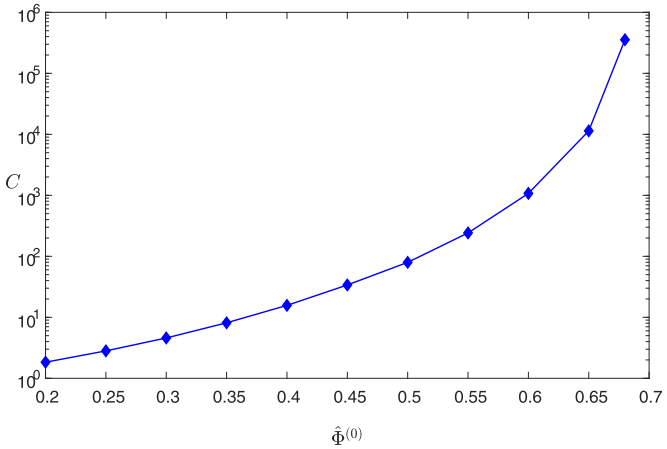

FIG. 3. The constant of integration, C, in Eq. (9) for the range of input concentration $\hat{\Phi}^{(0)}$.

these phenomena are linked to the particular input concentration distribution suggested in (16) and in Fig. 1.

The constant of integration, C, was obtained in Eq. (9) for the solution of $\Phi^{(1)}$ for all input cases spanning $0.2 \leqslant \hat{\Phi}^{(0)} \leqslant 0.65$. See Fig. 3. The results for $\Phi^{(1)}$ are of particular interest since it is associated with the local average particle size. Note that the values of C spans five orders of magnitude from $O(1)$ at low $\hat{\Phi}^{(0)}$ to $O(10^5)$ at high $\hat{\Phi}^{(0)}$.

In Fig. 4 below, we report stationary results for suspensions having initial particle concentrations in the range $0.2 \leqslant \hat{\Phi}^{(0)} \leqslant 0.65$. The results describe the following variables: $\Phi^{(0)}$, $\Phi^{(1)}$, $\bar{a}$, γ, μ, and u, all functions of r, and some particular parameters such as the change in pressure gradient and the maximum value of the mean size and its radial location in the tube cross section.

Several characteristics that evolved in the suspension are evident in the various stationary profiles depicted in Fig. 4. The first observation is that in all cases, particles are driven toward the center of the tube to result in $\Phi^{(0)} = \phi_m = 0.7$ there.

When initial concentration is extremely high, e.g., at $\hat{\Phi}^{(0)} = 0.65$, the resulting stationary concentration profile is reduced monotonically from its maximum value at $r = 0$ to a minimum value at $r = 1$. This is similar to what was observed for monodisperse suspensions (see, e.g., Hampton *et al.* [33]) though for less concentrated systems. In such profiles there exists an intermediate portion of the profile at $0 < r < 1$, where the resulting concentration is close to the initial one. But, when the results of the local average size, $\bar{a} = \Phi^{(1)}/\Phi^{(0)}$, are inspected it becomes clear that in the polydisperse suspension there is a relatively large $\bar{a}$ at the tube center, but also a considerable portion of large particles remains near the tube wall, while the minimum average size is found at $0 < r < 1$. Recall that the flux of particles is built at two opposite driving forces, defined by Leighton and Acrivos [8] to be the gradient of the concentration and the gradient of shear intensity, or translated by Phillips *et al.* [10] to be the gradient of interaction frequency and the gradient of the effective viscosity. Thus, the stationary profiles in the case $\hat{\Phi}^{(0)} = 0.65$ suggest that the competition of intensity of the two effects is being reversed somewhere along the radial direction, thereby leaving large particles also near $r = 1$.

In cases when the initial concentration is somewhat reduced but is still relatively high, say at $\hat{\Phi}^{(0)} = 0.6$ and $\hat{\Phi}^{(0)} = 0.55$, the profiles of the stationary concentration are still monotonically decreasing from $r = 0$ to $r = 1$, while the value of the average size shows a significant decrease near $r = 1$. Note that a minimum in $\Phi^{(0)}$ develops near $r = 1$. Furthermore, the maximum in the average size begins to deviate from the tube center at $r = 0$. The cases calculated for a further decrease in $\hat{\Phi}^{(0)}$, say at $\hat{\Phi}^{(0)} = 0.5$, $\hat{\Phi}^{(0)} = 0.45$, and $\hat{\Phi}^{(0)} = 0.4$, exhibit a further movement of the minimum of $\Phi^{(0)}$ away from the tube wall and of the maximum of $\bar{a}$ away from the tube center, as

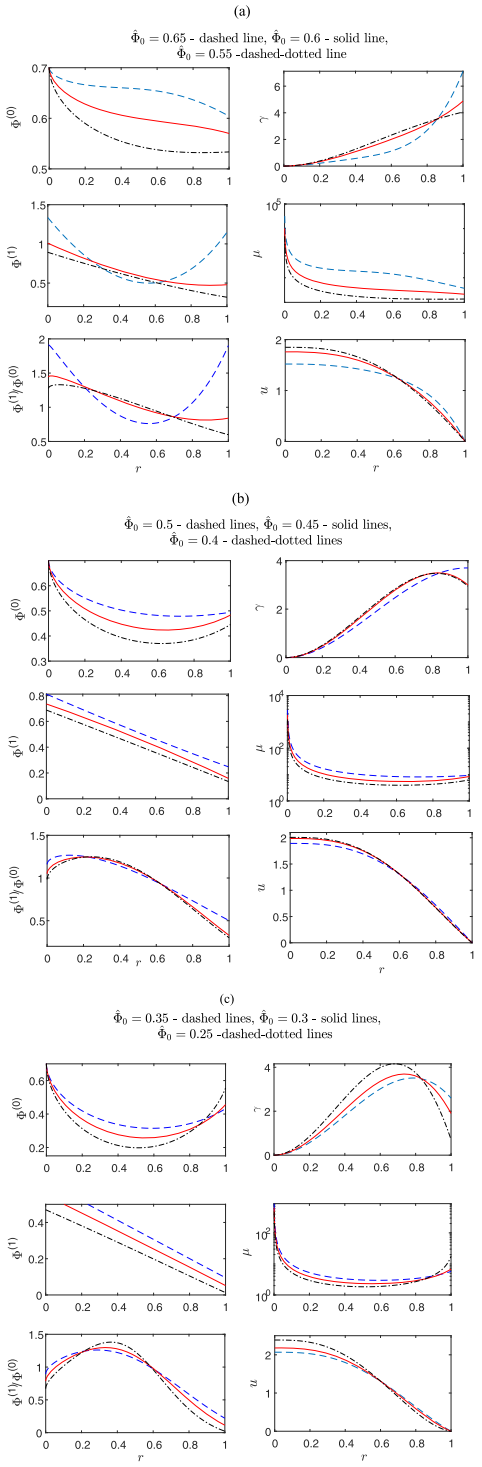

FIG. 4. Stationary profiles of $\Phi^{(0)}$, $\Phi^{(1)}$, $\bar{a} = \Phi^{(1)}/\Phi^{(0)}$, γ, μ, and u in the tube cross section. Cases (a)–(c) correspond to initial $\hat{\Phi}^{(0)}$ values of 0.65, 0.6, and 0.55; 0.5, 0.45, and 0.4; and 0.35, 0.3, and 0.25, respectively.

shown in Fig. 4 and in Table II below. Note that the moment $\Phi^{(1)}$ evolved to an almost linear profile decreasing from a maximum at $r = 0$ to a minimum at $r = 1$.

The increase of $\Phi^{(0)}$ near the tube wall is a direct result of the normal distribution depicted in Fig. 1, where very large particles and very small particles exist in the suspension in similar small amounts. Hence, while separating due to migration, with the large ones concentrated near the tube center and the small ones near the tube wall, they affect similarly the $\Phi^{(0)}$ profile while inversely the $\Phi^{(1)}$ and the associated $\bar{a}$ profiles. Furthermore, the finding of small increase of volume fraction near the tube wall is discussed in view of the finding of Di Vaira *et al.* [14], who reported on significant presence of large particles near the wall, where they were not expected. A small fraction of large particles can influence the local concentration distribution without significantly altering the average size.

D. Effective physical properties

The local effective viscosity, μ, being a unique function of $\Phi^{(0)}$, follows its profile changes. At high values of $\hat{\Phi}^{(0)}$ it is monotonically decreasing from the tube center toward the tube wall, exhibiting several orders of magnitude difference between the two regions. However, at reduced values of $\hat{\Phi}^{(0)}$, in cases where the resulting concentration profile, $\Phi^{(0)}$, exhibits a local minimum at some intermediate r, so does μ. Note that at relatively low values of $\hat{\Phi}^{(0)}$, say smaller than 0.45, the resulting concentration near $r = 1$ is considerably elevated and so is μ. This, in view of Eqs. (9) and (10), is reflected in the profiles of γ and u as is discussed further below.

The velocity gradient, γ, is considerably suppressed near $r = 0$ being of $O(r^2)$ there, as was suggested following (9) for all values of $\hat{\Phi}^{(0)}$. However, as is evident in Fig. 4, while in cases of high $\hat{\Phi}^{(0)}$ γ increases monotonically towards $r = 1$, in reduced $\hat{\Phi}^{(0)}$ cases, γ exhibits a maximum at some $r < 1$. In cases of low $\hat{\Phi}^{(0)}$ such a profile results in an inflection point that appears in the velocity profile. For example, in the case of $\hat{\Phi}^{(0)} = 0.25$ it is at about $r = 0.6$. It is noted that such a zero vorticity may become a source of velocity profile instability, which is typical for viscous boundary layers at high Reynolds number flows.

In general, the calculated results in Fig. 4 suggest that as $\hat{\Phi}^{(0)}$ decreases, two characteristics change monotonically at the tube center: the average particle size decreases and the maximum velocity increases. $\Phi^{(0)}$, μ, and γ are interconnected via the Krieger expression and Eq. (10). The system experiences a transition at some intermediate $\hat{\Phi}^{(0)}$, which is followed by an increase of the effective viscosity and a decrease of γ toward $r = 1$. Thus, this transition affects the respective gradients of these variables in the flux balance (6) and is reflected in the transition in the growth or reduction of higher moments discussed after Fig. 2.

In Fig. 5 we depict a comparison of the resulting velocity distributions in some of the cases described above. Recall that all profiles are normalized by the initial average Newtonian velocity distribution, $\hat{\bar{u}}$. Figure 5(a) shows the change of the profiles deviating from the Newtonian parabolic distribution for cases with $\hat{\Phi}^{(0)} \geqslant 0.45$. In these cases, the maximum velocity at the tube center decreases with the increase of particle volume concentration and the associated effective viscosity there. In Fig. 5(b) we focus on a comparison between the results corresponding to low, high, and middle values of the initial concentration $\hat{\Phi}^{(0)}$, with the initial Newtonian profile. When the particle concentration is high, at $\hat{\Phi}^{(0)} = 0.65$, the velocity profile near the tube center is flatter with a core at the center of an almost plug flow. Near the tube wall the viscosity is reduced and the velocity gradient is increased. These characteristics, are similar to the well-known results in monodisperse suspensions. They are typical of turbulent boundary-layer profiles and it is quite ironic that they are more pronounced when the flow becomes more creeping with a suspension that is ever more concentrated. When the particle initial concentration is relatively low, at $\hat{\Phi}^{(0)} = 0.25$, the maximum velocity is much higher than in the homogeneous Newtonian case, while the velocity gradient decreases. A transition between the above two cases, with a profile more similar to the Newtonian one, is typical of intermediate initial concentrations such as $\hat{\Phi}^{(0)} = 0.4$ or 0.45, with the latter depicted in the figure.

More characteristics and results are shown in Tables I and II below.

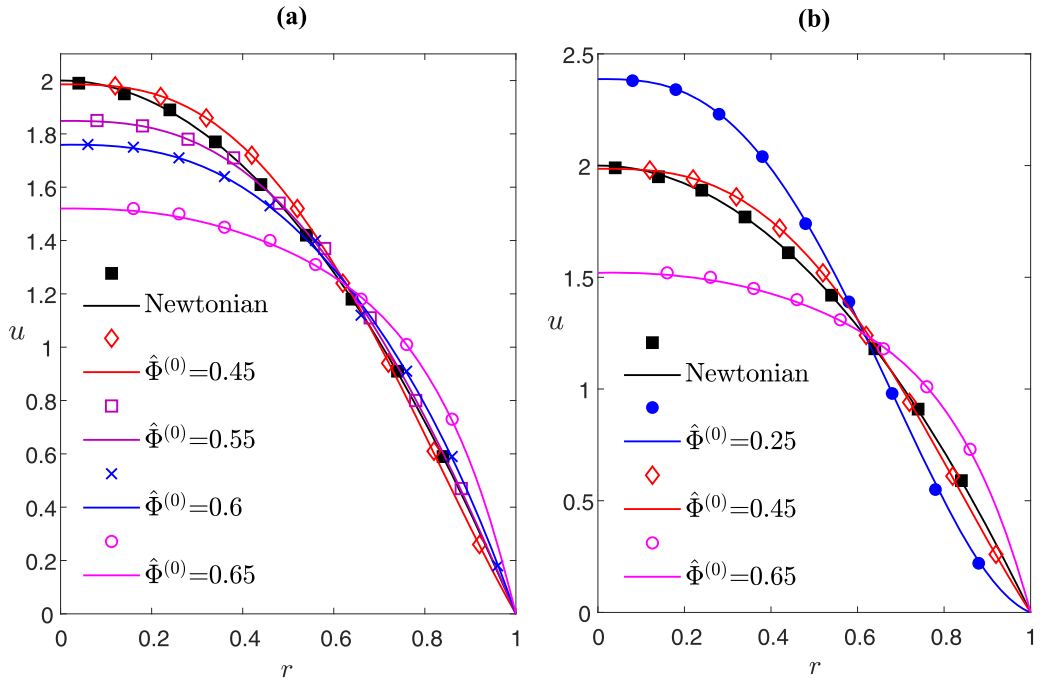

FIG. 5. Stationary velocity profiles: (a) Flattening profiles at $\hat{\Phi}^{(0)} \geqslant 0.45$ and (b) Comparison of at high, intermediate, and low particle concentration.

Tables I and II present a collection of some results concerning stationary physical and other characteristics resulting from the migration process. The first three rows in Table I correspond to the change in the axial pressure gradient required to maintain the flow, which is a manifestation of the viscous energy dissipation rate in the suspension. The first row depicts the calculated pressure gradient established after the migration achieved stationarity for each case of inlet concentration $\hat{\Phi}^{(0)}$, while the second row is the initial pressure gradient for the parabolic flow profile of the homogeneous suspension. Naturally, in both rows the lower is $\hat{\Phi}^{(0)}$ the lower is the pressure gradient. However, when observing the ratio between final and initial values it is evident that the trend of it is opposite, i.e., it is increasing with the decrease of $\hat{\Phi}^{(0)}$. Furthermore, in the cases with high values of $\hat{\Phi}^{(0)}$ the dissipation rate in the stationary profiles is reduced compared to that in the homogeneous suspensions introduced into the tube. However, in cases of relatively low $\hat{\Phi}^{(0)}$ the

TABLE I. A collection of results emerging from input of various inputs $\hat{\Phi}^{(0)}$ with the normal distribution of the form given in (16).

Input volume fraction, $\hat{\Phi}^{(0)}$	0.65	0.6	0.55	0.5	0.45	0.4	0.35	0.3	0.25	0.2
$(\frac{dP}{dz})$, Eq. (10)	531.2	209.2	110.9	68.9	50.6	37.1	29.8	25.9	24.1	21.9
$(\frac{d\hat{P}}{dz}) = 8\hat{\mu}$	975.1	276.2	132.0	78.2	52.1	37.4	28.3	22.2	17.9	14.8
$(\frac{dP}{dz})/(\frac{d\hat{P}}{dz})$	0.545	0.758	0.840	0.881	0.971	0.991	1.04	1.17	1.39	1.48
Maximum of velocity, $u_{\max}$ $(r = 0)$	1.520	1.759	1.849	1.892	1.986	2.006	2.068	2.179	2.387	2.458
C, Eq. (9)	11380	1075	241.7	79.60	33.90	15.68	8.123	4.584	2.815	1.584

TABLE II. A collection of results characterizing the distribution of the stationary concentration.

Input volume fraction, $\hat{\Phi}^{(0)}$	0.65	0.6	0.55	0.5	0.45	0.4	0.35	0.3	0.25	0.2
Maximum of mean size, $\bar{a}_{\max}$	1.909	1.459	1.329	1.268	1.246	1.248	1.26	1.3	1.38	1.53
Position r of $\bar{a}_{\max}$	0	0.015	0.06	0.125	0.21	0.243	0.29	0.33	0.36	0.38
Minimum of $\phi(r)$, $\phi_{\min} = \Phi^{(0)}_{\min}$	0.604	0.570	0.532	0.479	0.424	0.370	0.315	0.257	0.198	0.142
Position r of $\Phi^{(0)}_{\min}$	1.000	1.000	0.844	0.724	0.641	0.622	0.590	0.554	0.514	0.487
$\Phi^{(0)}(r = 1)$	0.604	0.570	0.534	0.495	0.483	0.446	0.432	0.457	0.555	0.551

trend is reversed and the stationary state dissipates more energy. The transition is at an intermediate initial concentration of about $\hat{\Phi}^{(0)} = 0.4$.

In the next row of Table I we give the numerical value of the maximum developed velocity of the profiles depicted in Fig. 5 which, naturally, is at the tube center. Note that the relatively low maximum increases as $\hat{\Phi}^{(0)}$ decreases, and that it surpasses the Newtonian value, $u_{\max} = 2$, at about $\hat{\Phi}^{(0)} \approx 0.4$.

Table I also shows the constant of integration in Eq. (9) corresponding to the moment $\hat{\Phi}^{(1)}$, which plays an important role in the calculation of the average particle size $\bar{a}$ at each r. As can be seen in Table II, $\bar{a}$ achieves a maximum, $\bar{a}_{\max}$, which is also declining in size as $\hat{\Phi}^{(0)}$ reduces in the range of relatively high $\hat{\Phi}^{(0)}$ values, but is increasing in size for values of $\hat{\Phi}^{(0)} < 0.4$. It appears that the case with $\hat{\Phi}^{(0)} \approx 0.4$ is a transition case and it can be correlated with the appearance of an inflection point in the stationary velocity profile and the onset of decline in the velocity gradient, γ, beyond its maximum value as it approaches the tube wall toward $r = 1$. The position of $\bar{a}_{\max}$ departs from the tube center and monotonically increases as $\hat{\Phi}^{(0)}$ decreases.

The last three rows of Table II depict particular values of the stationary distributions. The minimum value of $\Phi^{(0)}$ is monotonically increasing with respect to the increase in $\hat{\Phi}^{(0)}$, and its radial position approaches the tube wall as $\hat{\Phi}^{(0)}$ approaches its maximum. The bottom row in Table II contains the stationary concentration at the tube wall, $\Phi^{(0)}(r = 1)$, which also exhibits a minimum near $\hat{\Phi}^{(0)} \approx 0.4$.

We note, again, that the integral results described in this section correspond to the particular form of the initial normal (Gaussian) particle distribution functions given in (16). These results are associated with the postdispersion particle distributions discussed in Sec. V below.

V. STATIONARY PARTICLE DISTRIBUTIONS IN THE TUBE CROSS SECTION

A. The inverse problem

The task of finding local particle-size distribution requires solving parallel set of boundary integral equations for each radial location, r. These are of the form of integral equations of the first kind [Eq. (3)] for the distribution moments. In the sections above we described an approximation for the first ten moments that implies truncation to the finite set:

$$\Phi^{(n)}_{(\text{apprx})} = \int_{a_{\min}}^{a_{\max}} a^n \phi(a) da, \quad 0 \leqslant n \leqslant N = 9, \tag{19}$$

Where $\Phi^{(n)}_{(\text{apprx})}$ are the solutions of $\Phi^{(0)}$, $\Phi^{(1)}$, and $\Phi^{(n+1)}$ given by Eqs. (20), (9), and (17), respectively, with explicit examples given in Figs. 2–4. This becomes just another typical example of the familiar inverse problem of mathematical physics, in this case a linear one. In such problems a full spectrum or distribution is calculated from a finite set of observations. Examples of applications are in medical imaging, computer vision, geophysics, oil and water drilling, and many other problems involving stability, regularization, and model discretization in infinite dimension. This field is beyond the scope of this paper and the interested reader is referred to several books and journals

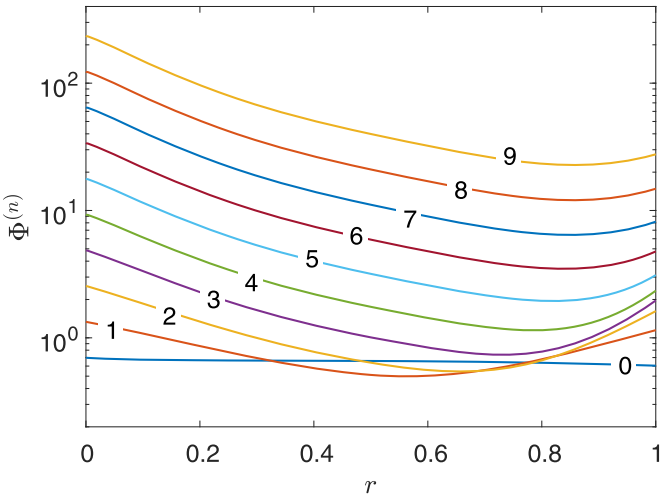

FIG. 6. A logarithmic plot of stationary moments obtained for high-input particle concentration at $\hat{\Phi}^{(0)} = 0.65$.

that address the subject (see, e.g., *Journal of Inverse and Ill-Posed Problems*; also *Inverse Problems in Science and Engineering*, and several books by De Gruyter and other publishers).

One simple method to find a continuous distribution from the finite number of moments is to discretize the distribution and invert the matrix of coefficients at each r. However, when the number of moments $N \gg 1$ the ratio $\hat{\Phi}^{(N)}/\hat{\Phi}^{(N-1)}$ approaches a constant. In such cases the matrix may become pseudosingular and irrelevant homogeneous solutions can contaminate the desired distribution. This is evident even in the limited number of ten moments, $N = 9$, which we discussed above. The logarithmic plot of Fig. 2(a), shown below in Fig. 6, suggests visually the similarity of the differences in $\log\left(\frac{\hat{\Phi}^{(9)}}{\hat{\Phi}^{(8)}}\right)$ and $\log\left(\frac{\hat{\Phi}^{(8)}}{\hat{\Phi}^{(7)}}\right)$ that can be equal at some radial location r.

To demonstrate this, in Fig. 7 we depict plots of the ratio $\frac{\Phi^{(9)}}{\Phi^{(8)}}/\frac{\Phi^{(8)}}{\Phi^{(7)}}$ for the cases $0.25 \leqslant \hat{\Phi}^{(0)} \leqslant 0.65$. Indeed, in all cases, we see that the ratio is very close to unity in the entire cross section. It is equal to 1 at the tube center, and only slightly monotonically deviates from unity to a maximum of a couple of percent along the entire tube radius.

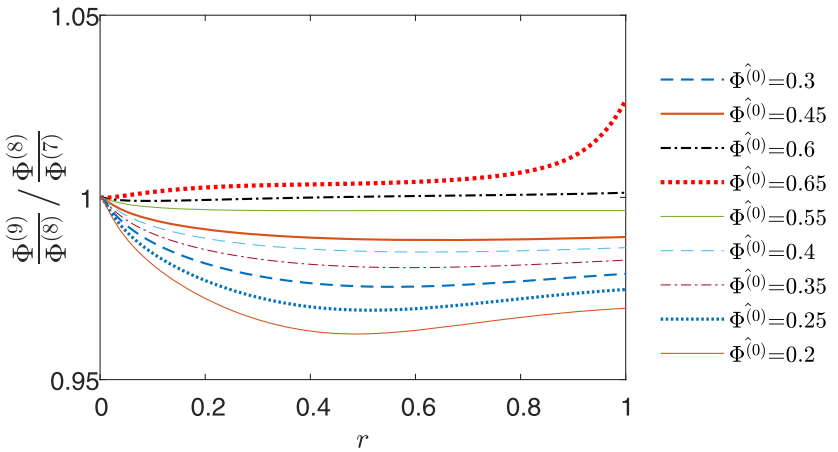

FIG. 7. The deviation from unity for sequential moment ratios.

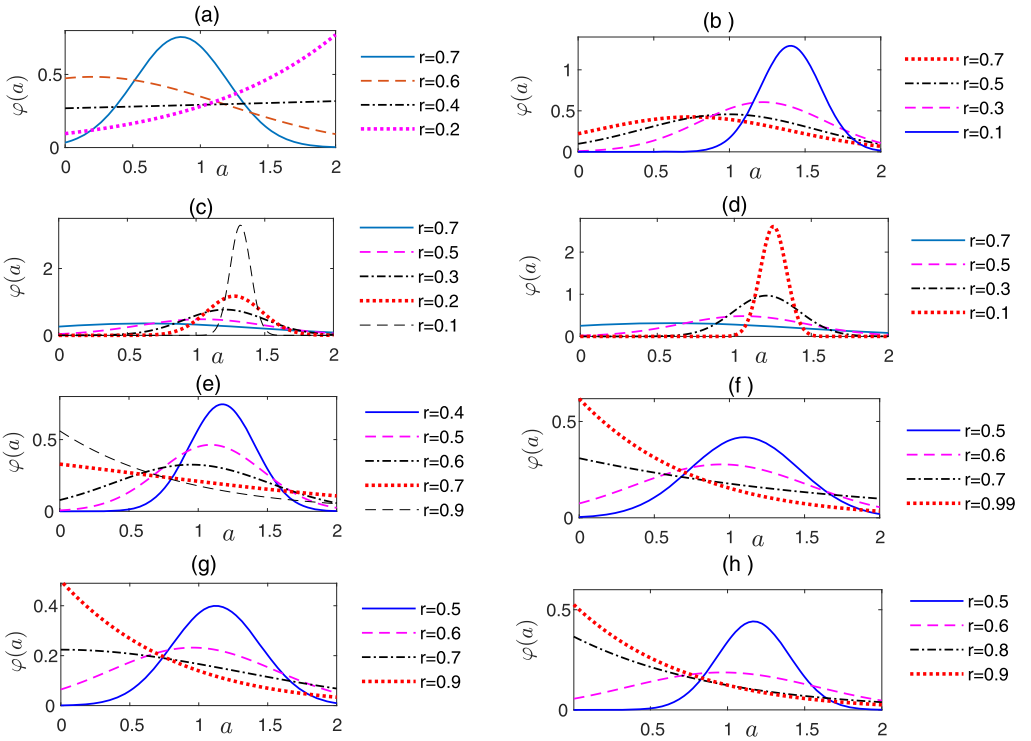

FIG. 8. Stationary particle-size distributions of, $\phi(a)$, in various radial locations. Cases (a)–(h) correspond to initial uniform $\hat{\Phi}^{(0)}$ values of 0.65, 0.6, 0.55, 0.5, 0.45, 0.4, 0.35, and 0.3, respectively.

B. Local size distributions

Instead of resorting to truncation methods, for the sake of simplicity, we assume that at each r the local particle-size distribution is a segment of a normal size distribution that has the form

$$\tilde{\phi}(a, r) = \beta_1 e^{-\beta_2 (a-\beta_3)^2}, \quad 0 < a < 2 \tag{20}$$

where β_1, β_2, and β_3 are parameters to be determined for each particular location, r. Integration over a provides explicit expressions for the various moments $\tilde{\Phi}^{(n)}$ being functions of the β_k, $k = 1, 2,$ and 3. We then sum the squares of the differences of these functions and corresponding moments to the form

$$S = \sum_{n=0}^{N} (\tilde{\Phi}^{(n)} - \Phi^{(n)})^2, \tag{21}$$

and minimize this sum by applying the *fmincon* operator that is available in the MATLAB toolbox, using the constraints $\beta_k > 0$.

In Fig. 8, below, we depict typical results of stationary particle-size distributions $\phi(a)$ at various radial positions, for various values of the initial homogeneous particle-size distributions, $\hat{\phi}(a)$, corresponding to concentrations $\Phi(r)$ at these locations reported in Fig. 4.

We open the discussion of the various plots in Fig. 8 by indicating the results that are expected from the similarity of the process to the ones already established for monodispersed or multi-dispersed suspensions (see, e.g., Refs. [10,23]). Clearly, large particles migrate toward the tube center, a region with a relative low shear rate, γ, and small particles migrate toward the tube wall where the shear is high. This migration is balanced by counterfluxes associated with gradients of

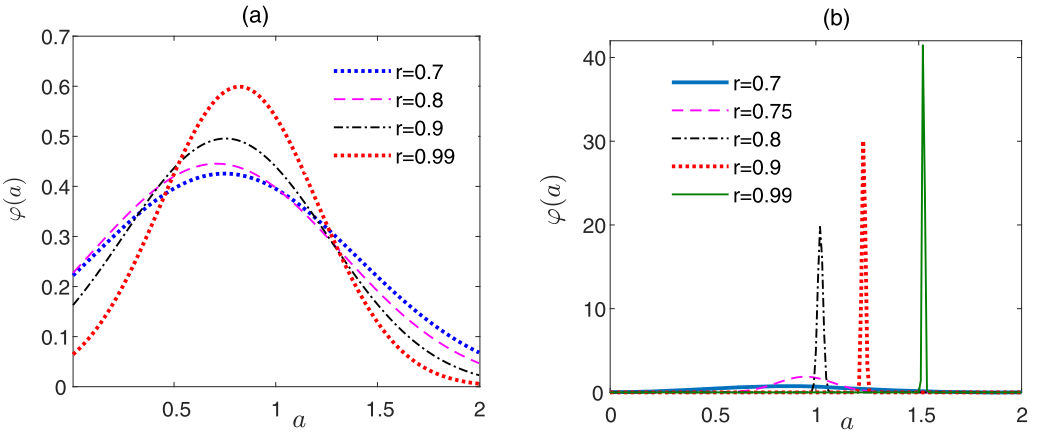

FIG. 9. Particles-size profiles at positions close to the tube wall: (a) $\hat{\Phi}^{(0)} = 0.6$ and (b) $\hat{\Phi}^{(0)} = 0.65$.

respective concentration changes. Thus, examples of large particles' dominant presence can be seen in profiles at $r \leqslant 0.5$ depicted in Figs. 8(a)–8(h). Similarly, a buildup of relative presence of smaller particles is shown at $r \geqslant 0.6$. In between we observe local profiles that include a central size of maximum concentration, with a normal distribution about it. These profiles shift position as the initial concentration, $\hat{\Phi}^{(0)}$, varies.

Near the tube center there is a dominant presence of large particles and a depleted presence of small particles. On the other hand, near the tube wall there exist a dominant presence of small particles and a reduced presence of large particles. Furthermore, since the large and small particles migrate to the opposite directions, the middle region of the tube radius contains only meager portions of these sizes. Thus, the results displayed in Fig. 8 and in the following section support the assumption adopted in Secs. III and IV that in the stationary state, the change in ϕ_m is small and can be approximated by a constant increase of few percent.

C. Some particular distributions near the tube center and wall

There are certain eccentric results associated with the competition between the change of the total concentration at some location and the existence of a profile including all sizes there. When the initial total concentration is relatively high, e.g., $\hat{\Phi}^{(0)} = 0.6$, it is shown in Fig. 4(b) that the three values of $\Phi^{(0)}$, $\Phi^{(1)}$ and $\bar{a}$, near the tube wall are reduced, as would be naturally expected. Indeed, the particle-size profiles depicted in Fig. 9(a) are centered at $a < 1$, at positions as close as $r = 0.99$. However, when the initial concentration is higher and close to the maximum value, say $\hat{\Phi}^{(0)} = 0.65$, Fig. 4(a) indicates that although $\Phi^{(0)}$ is reduced, the values of $\Phi^{(1)}$ and $\bar{a}$ remain relatively high, suggesting different particle-size profiles in the region near the wall. The latter are depicted in Fig. 9(b) showing near-singular isolated profiles of relatively high particle sizes in that region, fractions that did not migrate toward the center of the tube.

When $\hat{\Phi}^{(0)}$ is relatively low we encounter opposite phenomena near the tube center. The typical characteristics of the moment distributions that are evident in such cases [see, e.g., Figs. 4(g) and 4(h)] are that the location of $\bar{a}$ is far from the tube center, the $\Phi^{(0)}$ and the effective viscosity profile have minima far from the tube wall, and the gradient of γ changed sign at some intermediate position. In such cases near-singular particle-size distributions, with typical maximum particle size near the initial average ($\hat{a} \approx 1$), are evident near the tube center, as close as $r = 0.01$. Such profiles are depicted in Fig. 10 for the cases $\hat{\Phi}^{(0)} = 0.3$ and $\hat{\Phi}^{(0)} = 0.35$, and a similar result exists for $\hat{\Phi}^{(0)} = 0.4$.

The opposite, almost singular, fractionation of particle-size distributions near the tube wall and center, for high and low initial $\hat{\Phi}^{(0)}$, respectively, suggests the existence of transition in the

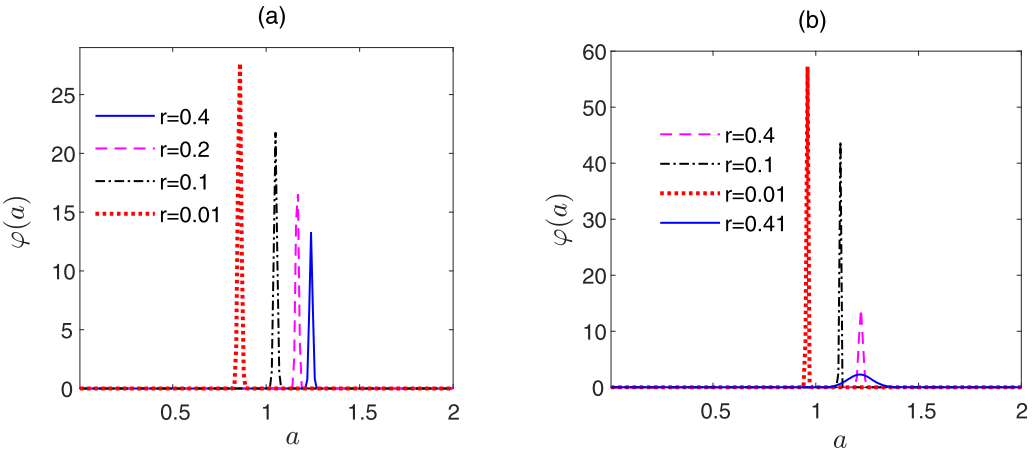

FIG. 10. Particle-size profiles at positions close to the tube center: (a) $\hat{\Phi}^{(0)} = 0.3$ and (b) $\hat{\Phi}^{(0)} = 0.35$.

suspension migration behavior at some value of initial concentration. Figures 2(a) and 2(c) show that values of sequential moments advance differently in the case of high and low initial $\hat{\Phi}^{(0)}$, increase in the former case and decrease in the latter one, while they keep similar orders of magnitude near $\hat{\Phi}^{(0)} = 0.4$. In addition, Table I suggests that the resulting pressure gradient for flow maintenance is gradually increasing and surpasses the initial Newtonian one at about $\hat{\Phi}^{(0)} = 0.4$. Furthermore, Table II shows a minimum in the location of $\bar{a}_{\max}$ near $\hat{\Phi}^{(0)} = 0.45$, while Fig. 4 depicts the existence of a maximum in γ for $\hat{\Phi}^{(0)} \leqslant 0.45$ at some intermediate positions $r < 1$, and a change in the direction of migration driving forces [recall Eq. (9)]. These results are corroborated by the similarity of particle-size distributions for $\hat{\Phi}^{(0)} \leqslant 0.45$, all centered around a similar $a_{\max}$ at intermediate values of r, as is shown in Fig. 11.

We conclude this section by examining the results at the center of the tube. The profiles suggested in Eq. (20) and the minimization algorithm applied in (21) at the center provide an almost unique particle size for each choice of $\hat{\Phi}^{(0)}$, in the form of a Dirac delta function. These obtained results

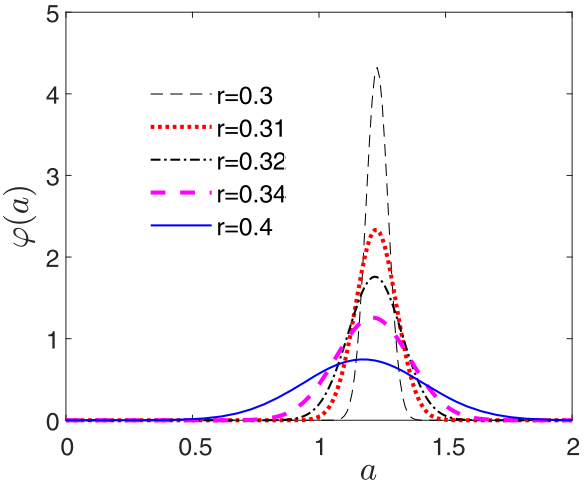

FIG. 11. Particle-size distributions about $a_{\max} \approx 1.2$ at intermediate r positions, $\hat{\Phi}^{(0)} = 0.45$.

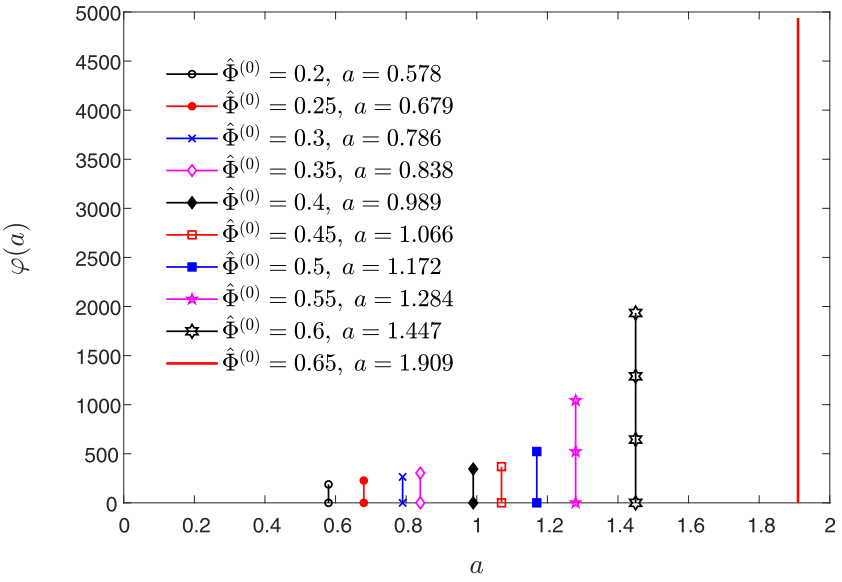

FIG. 12. Particle sizes at $r = 0$ for the various cases of $\hat{\Phi}^{(0)}$. The minimum obtained for S in Eq. (21) is of $O\,(10^{-11})$.

suggest that the concentration at $r = 0$ involves particles of only one size. These sizes are depicted in Fig. 12 for the tested cases.

It is noted that the very steep normal distributions shown in Figs. 9–11 are almost completely devoid of large and small particle sizes and, hence, at these locations the values of ϕ_m are very close to the respective monodispersed cases. This numerically singular result is in an agreement with

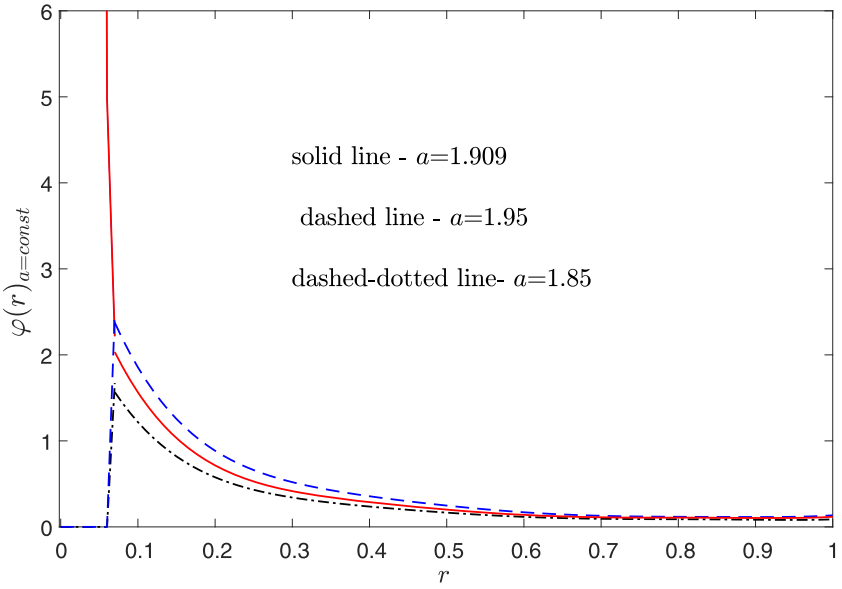

FIG. 13. The concentration distributions of sizes 1.95, 1,909, 1.85 near the tube center $r \to 0$ in the case $\hat{\Phi}^{(0)} = 0.65$.

what can be calculated for a suspension containing several discrete particle sizes by expanding the expressions of Shauly *et al.* [23] at $r \to 0$, and by direct manipulation of their Eq. (2). Furthermore, in the absence of a rigorous proof when the particle size distribution is continuous; an example is shown in Fig. 13. There, a calculation of the concentration distributions of three sizes, $a = 1.909$, 1.95, and 1.85 near $r = 0$ in the case $\hat{\Phi}^{(0)} = 0.65$, demonstrates that the concentrations of both sizes, larger and smaller than 1.909, are pushed away from the center to start ascending at about $r = 0.06$. Note the difference in scales of the ordinates in Figs. 12 and 13.

VI. CONCLUDING REMARKS

In this paper we have established a method of studying shear-induced migration of particles in a viscous suspension that contains a continuous particle-size distribution. The method follows the definition of Phillips *et al.* [10], which considered migration due to gradients in particles' interaction frequency and shear-flow intensity. The problem is converted to evolution of infinite number of moments of the particles' concentration. For a stationary flow in a circular tube, the need to truncate the number of moments is replaced by assuming an objective function and minimizing its deviation with respect to a finite number of moments to satisfy a chosen accuracy.

The particular suspension considered contained a normal distribution of particle sizes. Several initial particles' volume concentrations were considered, ranging from 0.2 to 0.65. The algorithm provided integral stationary results of ten moments and their distribution in the tube cross section. These are provided in conjunction with profiles of particle concentration, average particle size, effective viscosity, shear intensity, and velocity.

Particle-size distributions are obtained from the moments by optimizing a three-parameter approximation for each case at each radial position. The detailed results shown in this work apply solely to the assumed normal particle-size distribution that existed before migration. Each particular initial distribution should be handled separately and would provide different moments and particle distributions, and their consequences. In this case of normal input distribution, we encountered two main regions of results depending on the initial particle concentrations. For relatively high initial concentration, the dependence of the established total concentration (the zero moment) on the radial position and the flow characteristics are qualitatively similar to those encountered in monodisperse suspensions by the various methods cited in the Introduction. On the other hand, for lower-input concentrations the zero moment may exhibit a pronounced elevation at the wall of the tube, while the average particle size keeps reducing to a minimum there. This effect was not observed for monodisperse systems. Another unexpected result with this input particle-size distribution suggests cases in which there exist regions of isolated sizes, either near the tube center or close to the tube wall. These regions may be useful toward separation of sizes when other methods cannot provide it. The regions of isolated particles were found previously for bidisperse suspensions in Ref. [23]. Note that in general, the results for particle-size distributions of polydisperse systems along the tube radius are, and should be, different from those expected with monodisperse case. They depend on additional effects and factors such as size separation and input profiles. Indeed, the predictions in our work, particularly the unexpected ones mentioned above that deviate from monodisperse systems, are still waiting for corroboration by experimental results.

ACKNOWLEDGMENT

This work is supported by Israel Science Foundation (IL) 419/22.

[1] A. Karnis, H. L. Goldsmith, and S. G. Mason, The kinetics of flowing dispersions. I. Concentrated suspensions of rigid particles, J. Colloid Interface Sci. **22**, 531 (1966).

[2] F. Gadala-Maria and A. Acrivos, Shear-induced structure in a concentrated suspension of solid spheres, J. Rheol. **24**, 799 (1980).
[3] D. Leighton and A. Acrivos, Measurement of shear-induced self-diffusion in concentrated suspensions of spheres, J. Fluid Mech. **177**, 109 (1987).
[4] D. M. Kalyon, Apparent slip and viscoelasticity of concentrated suspensions, J. Rheol. **49**, 621 (2005).
[5] D. M. Kalyon, Rheological behavior of concentrated suspensions as affected by the dynamics of the mixing process, Rheol. Acta **45**, 641 (2006).
[6] J. R. Abbott, N. Tetlow, A. L. Graham, S. A. Altobelli, E. Fukushima, L. A. Mondy, and T. S. Stephens, Experimental observations of particle migration in concentrated suspensions: Couette flow, J. Rheol. **35**, 773 (1991).
[7] G. P. Krishnan, S. Beimfohr, and D. T. Leighton, Shear-induced radial segregation in bidisperse suspensions, J. Fluid Mech. **321**, 371 (1996).
[8] D. Leighton and A. Acrivos, The shear-induced migration of particles in concentrated suspensions, J. Fluid Mech. **181**, 415 (1987).
[9] E. C. Eckstein, D. G. Bailey, and A. H. Shapiro, Self-diffusion of particles in shear flow of suspensions, J. Fluid Mech. **79**, 191 (1977).
[10] R. J. Phillips, R. C. Armstrong, R. A. Brown, A. L. Graham, and J. R. Abbott, A constitutive equation for concentrated suspensions that accounts for shear-induced particle migration, Phys. Fluids A **4**, 30 (1992).
[11] P. R. Nott and J. F. Brady, Pressure-driven flow of suspensions: Simulation and theory, J. Fluid Mech. **275**, 157 (1994).
[12] A. M. Leshansky, J. F. Morris, and J. F. Brady, Collective diffusion in sheared colloidal suspensions, J. Fluid Mech. **597**, 305 (2008).
[13] B. Chun, L. Kwon, H. W. Jung, and J. C. Hyun, Lattice Boltzmann simulation of shear-induced particle migration in plane Couette–Poiseuille flow: Local ordering of suspension, Phys. Fluids **29**, 121605 (2017).
[14] N. J. Di Vaira, Ł. Łaniewski-Wołłk, R. L. Johnson Jr., S. M. Aminossadati, and C. R. Leonardi, Influence of particle polydispersity on bulk migration and size segregation in channel flows, J. Fluid Mech. **939**, A30 (2022).
[15] R. H. Davis, Hydrodynamic diffusion of suspended particles. A symposium, J. Fluid Mech. **310**, 325 (1996).
[16] J. J. Stickel and R. L. Powell, Fluid mechanics and rheology of dense suspensions, Ann. Rev. Fluid Mech. **37**, 129 (2005).
[17] R. M. Klaver and C. G. P. H. Schroen, A review of shear-induced particle migration for enhanced filtration and fractionation, in *Modeling Food Processing Operations*, edited by S. Bakalis, K. Knoerzer, and P. J. Fryer (Elsevier, Amsterdam, 2015), pp. 211–233.
[18] J. F. Morris, Toward a fluid mechanics of suspensions, Phys. Rev. Fluids **5**, 110519 (2020).
[19] C. Kang and P. Mirbod, Shear-induced particle migration of semi-dilute and concentrated Brownian suspensions in both Poiseuille and circular Couette flow, Int. J. Multiphase Flow **126**, 103239 (2020).
[20] A. Shauly, A. Wachs, and A. Nir, Shear-induced particle resuspension in settling polydisperse concentrated suspension, Int. J. Multiphase Flow **26**, 1 (2000).
[21] A. Acrivos, R. Mauri, and X. Fan, Shear-induced resuspension in a Couette device, Int. J. Multiphase Flow **19**, 797 (1993).
[22] A. Tripathi and A. Acrivos, Viscous resuspension in a bidensity suspension, Int. J. Multiphase Flow **25**, 1 (1998).
[23] A. Shauly, A. Wachs, and A. Nir, Shear-induced particle migration in a polydisperse concentrated suspension, J. Rheol. **42**, 1329 (1998).
[24] C. J. Koh, P. Hookham, and L. G. Leal, An experimental investigation of concentrated suspension flows in a rectangular channel, J. Fluid Mech. **266**, 1 (1994).
[25] N. Tetlow, A. L. Graham, M. S. Ingber, S. R. Subia, L. A. Mondy, and S. A. Altobelli, Particle migration in a Couette apparatus: Experiment and modeling, J. Rheol. **42**, 307 (1998).
[26] S. Pednekar, J. Chun, and J. F. Morris, Bidisperse and polydisperse suspension rheology at large solid fraction, J. Rheol. **62**, 513 (2018).
[27] I. M. Krieger, Rheology of monodisperse latices, Adv. Colloid Interface Sci. **3**, 111 (1972).

[28] G. P. Krishnan and D. T. Leighton, Dynamic viscous resuspension of bidisperse suspensions—I. Effective diffusivity, Int. J. Multiphase Flow **21**, 721 (1995).
[29] R. F. Probstein, M. Z. Sengun, and T.-C. Tseng, Bimodal model of concentrated suspension viscosity for distributed particle sizes, J. Rheol. **38**, 811 (1994).
[30] K. W. Desmond and E. R. Weeks, Influence of particle size distribution on random close packing of spheres, Phys. Rev. E **90**, 022204 (2014).
[31] A. Santos, S. B. Yuste, M. López de Haro, G. Odriozola, and V. Ogarko, Simple effective rule to estimate the jamming packing fraction of polydisperse hard spheres, Phys. Rev. E **89**, 040302(R) (2014).
[32] R. B. Reboucas, A. Z. Zinchenko, and M. Loewenberg, A pairwise hydrodynamic theory for flow-induced particle transport in shear and pressure-driven flows, J. Fluid Mech **952**, A2 (2022).
[33] R. E.Hampton, A. A. Mammoli, A. L. Graham, N. Tetlow, and S. A. Altobelli, Migration of particles undergoing pressure-driven flow in a circular conduit, J. Rheol. **41**, 621 (1997).